Laser dimpling process parameters selection and optimization using surrogate-driven process capability space

Erkan Caner Ozkat* [(a)], Pasquale Franciosa[(a)], Dariusz Ceglarek[(a)]
[(a)] Warwick Manufacturing Group, University of Warwick, Gibbet Hill Rd., Coventry CV4 7AL, UK
E – mail: E.C.Ozkat@warwick.ac.uk, P.Franciosa@warwick.ac.uk, D.J.Ceglarek@warwick.ac.uk

*Corresponding Author: Erkan Caner Ozkat (E.C.Ozkat@warwick.ac.uk, +44 (0) 2476573422)

Abstract

Remote laser welding technology offers opportunities for high production throughput at a competitive cost. However, the remote laser welding process of zinc-coated sheet metal parts in lap joint configuration poses a challenge due to the difference between the melting temperature of the steel (~1500 °C) and the vaporizing temperature of the zinc (~907 °C). In fact, the zinc layer at the faying surface is vaporized and the vapour might be trapped within the melting pool leading to weld defects. Various solutions have been proposed to overcome this problem over the years. Among them, laser dimpling has been adopted by manufacturers because of its flexibility and effectiveness along with its cost advantages. In essence, the dimple works as a spacer between the two sheets in lap joint and allows the zinc vapour escape during welding process, thereby preventing weld defects. However, there is a lack of comprehensive characterization of dimpling process for effective implementation in real manufacturing system taking into consideration inherent changes in variability of process parameters. This paper introduces a methodology to develop (i) surrogate model for dimpling process characterization considering multiple–inputs (i.e. key control characteristics) and multiple–outputs (i.e. key performance indicators) system by conducting physical experimentation and using multivariate adaptive regression splines; (ii) process capability space (C_p–Space) based on the developed surrogate model that allows the estimation of a desired process fallout rate in the case of violation of process requirements in the presence of stochastic variation; and, (iii) selection and optimization of the process parameters based on the process capability space. The proposed methodology provides a unique capability to: (i) simulate the effect of process variation as generated by manufacturing process; (ii) model quality requirements with multiple and coupled quality requirements; and (iii) optimize process parameters under competing quality requirements such as maximizing the dimple height while minimizing the dimple lower surface area.

Keywords Laser dimpling · Zinc coated steel · Surrogate modelling · Design of experiment · Multivariate adaptive regression splines · Process capability space

Nomenclature

D_H	Dimple height
D_U	Dimple upper surface area
D_L	Dimple lower surface area
S_s	Scanning speed
α	Incidence angle
F_O	Focal offset
L_T	Laser track
$KCCs$	Key Control Characteristics
$KPIs$	Key Performance Indicators
N_i	Number of KCCs
N_j	Number of KPIs
N_k	Number of experimental configurations
N_l	Number of experiment replications
d	Number of dependent KPIs
$N_s^{(k)}$	Number of KPIs in the k^{th} experimental configuration
$KCC_i^{(k)}$	i^{th} KCC value in the k^{th} experimental configuration
$KPI_j^{(k,l)}$	j^{th} KPI value in the k^{th} experimental configuration at the l^{th} replication
$\mu_{KPI_j^{(k)}}$	Mean value of the j^{th} KPI in the k^{th} experimental configuration
$\sigma_{KPI_j^{(k)}}$	Standard deviation of the j^{th} KPI in the k^{th} experimental configuration
$\hat{\mu}_{KPI_j}$	Estimated mean value of the j^{th} KPI
$\xi_{KPI_j^{(k)}}$	Success rate of the j^{th} KPI in the k^{th} experimental configuration
$\xi_{KPI_1^{(k)}\cdots KPI_d^{(k)}}$	Success rate of the dependent KPIs in the k^{th} experimental configuration
$\hat{\xi}_{KPI_j}$	Estimated success rate of the j^{th} KPI
$\hat{\xi}_{KPI_1\cdots KPI_d}$	Estimated success rate of dependent KPIs
$F_{\mu_{KPI_j}}$	Deterministic surrogate model of the j^{th} KPI
$F_{\xi_{KPI_j}}$	Stochastic surrogate model of the j^{th} KPI
$F_{\xi_{KPI_1\cdots KPI_d}}$	Stochastic surrogate model of dependent KPIs
PDF	Probability density function
SR	Success rate
β	Minimal desirable success rate
LL	Lower limit
UL	Upper limit
$\mathrm{KCC}-\mathrm{space}$	Process parameter space
$\mathbf{C_p - space}$	Process capability space
$\mathbf{DC_{p_j}}$ **– Space**	Deterministic process capability space of j^{th} KPI
$\mathbf{SC_{p_j}}$ **– Space**	Stochastic process capability space of j^{th} KPI
$\mathbf{DC_p}$ **– Space**	Deterministic process capability space
$\mathbf{SC_p}$ **– Space**	Stochastic process capability space

1. Introduction

Thin zinc coated steel sheets are widely used in the automotive industry due to its high corrosion resistance, especially in body-in-white and closure panels [1,2]. With the advancement of the laser technology, laser welding has been gradually replacing traditional welding methods since it offers cheaper and faster manufacturing process as well as better mechanical and aesthetic joint quality [3–5]. Despite such benefits, it is nonetheless challenging to achieve high quality joint in lap joint configuration of zinc coated steel since the boiling point of zinc (~907 °C) is significantly lower than the melting point of steel (~1500 °C), resulting in highly pressurized zinc vapour on the faying surfaces during the welding process. Left unaddressed, such zinc vapour can easily be trapped inside the molten pool which can lead to welding defects such as porosity, spatter, burn-through, and severe undercuts [6,7].

Over the past few years, significant amount of researches have been conducted to prevent the molten pool from being destroyed by the zinc vapour and several solutions have been proposed which can be classified as:

- *Ventilation* – This method is based on degasification of zinc vapour from the medium without causing any weld defects either by enlarging molten pool [8,9]; stabilizing the keyhole by employing shielding gas [10,11]; creating pre-drilled ventilation channels [12]; applying appropriate spacers at the faying surfaces [13–15]; or adopting a suction method to remove the vapour [16];
- *Inserting a thin metal foil* – This involves adding another material (e.g. Al & Cu) into the faying surface which absorbs zinc vapour or reacts with zinc vapour in such a way that a liquid alloy with a high boiling point is formed [17,18];
- *Tandem beams* – This approach employs a dual laser beam or a secondary heat source. The first beam applies pre-heating which vaporizes zinc coating and second beam performs actual welding [19–21];
- *Controlling keyhole oscillation* – The molten pool shape can be controlled based on the pulsed wave mode of laser beam so that more stable keyhole oscillation can be achieved, allowing the zinc vapour to escape during the keyhole closure [22,23]
- *Surf-sculpt* – This method creates surface features from the base metal by repeated movement of the low power on-focus laser beam in a short distance. These features increase surface area of the material and can be utilized as a spacer between the faying surface in lap joint [24,25].

All of the above solutions have been shown to produce satisfactory welds in lap joint configuration. However, they do have number of disadvantages due to: (*i*) challenges in development of system automation for robotic joining process (see *inserting a thin metal foil* solution); (*ii*) increased system complexity (see *ventilation* and *tandem beam* solutions) due to the need for installation of additional equipment which increases processing cost as well; and, (*iii*) increased cycle time (see *tandem beam*, *controlling keyhole oscillation* and *surf-sculpt* solutions) due to lower processing speed.

A promising technique for mitigation of zinc vapour is "*laser dimpling*" which makes a dimple on the faying surface of the upper sheet metal by rapid and single movement of the laser beam. Hence, the zinc vapour is vented out through the generated gap between the faying surfaces which is illustrated in Fig. 1. The laser dimpling process has been used by the automotive industry as it does not require any additional equipment and can be performed using the same laser source and fixture adopted for welding [26,27]. Furthermore, it is not restricted by the shape and curvature of the workpiece and weld location.

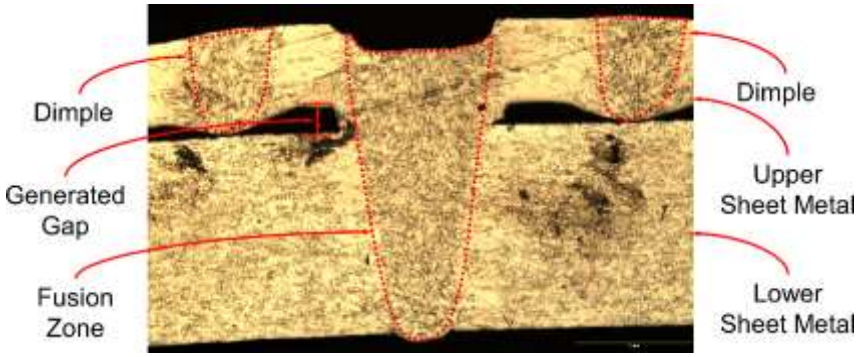

Fig. 1. Micro-section of laser welded joint with laser dimpling technique

The physical principle behind laser dimpling process can be explained by the "*humping effect*" which is influenced by the heat and mass transfer in the molten pool. In general, humps occur periodically along the weld bead which deteriorate the homogeneity of molten pool. In laser welding process, when the beam hits the workpiece, it creates a deep narrow cavity, known as keyhole. While laser beam is moving, the liquid material at the bottom of the keyhole flows upwards to the rear of the molten pool and generates a backward trail of a thin jet due to the surface tension on the keyhole walls. The solidification of this jet on the surface forms the hump at the rear and leading to a valley of cavity at the front which is given in Fig. 2. There has been significant research which look at the humping effect as a negative phenomenon during joining process, explained causes of humping effect and described ways to suppress the occurrence of

the hump [28–32]. However, the "*humping effect*" can be beneficially utilized by laser dimpling process to create the required gap in lap welding of zinc coated steels.

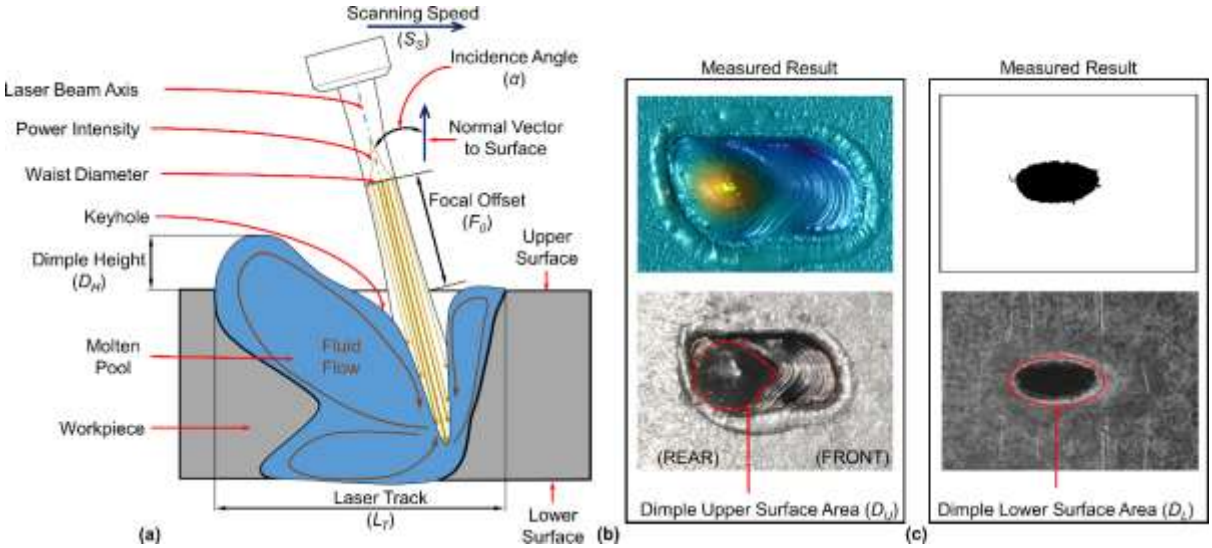

Fig. 2. (a) Illustration of humping effect during a dimpling process **(b)** dimple upper surface **(c)** dimple lower surface

According to Gu [26,27], humping effect was used to generate dimple for laser welding process first, by studying the influence of a single parameter, focal offset, on the dimple height. Then, they used this information to generate dimples at different scanning speed and incidence angle, while other parameters such as focal offset were kept constant. Results indicated that dimple height monotonically decreased with increasing both scanning speed and incidence angle; whereas, the dimple height firstly, increased and then decreased whilst increasing the focal offset. In a more recent study conducted by Colombo and Previtali [33] applied univariate linear regression model to determine influence of scanning speed on the dimple height keeping constant laser power, focal offset, and laser track. They found that linear energy, which is the amount of the energy supplied per unit time, was the primary factor affecting the dimple height. However, this study has limitation as authors considered only the influence of a single process parameter without exploring other important process parameters and their interactions.

The existing literature has focussed mainly on single–input (i.e. scanning speed) and single–output (i.e. dimple height) scenario which is necessary but not sufficient to give a complete characterisation of the dimpling process. Furthermore, the laser material processes are characterized as multiple–inputs and multiple–outputs (MIMO) system with non-linear functional relationship [34–36].

Thus, it is important to take into consideration MIMO–based scenario for dimpling process. It was observed in this paper that it is important to include the following multiple–inputs

parameters for a dimpling process: scanning speed (S_S), focal offset (F_O), incidence angle (α); and, laser track (L_T) as well as the following three key performance indicators (*KPIs*) to be addressed as multiple–outputs parameters: dimple height (D_H), dimple upper surface area (D_U); and, dimple lower surface area (D_L).

Another limitation associated with the current literature is the lack of modelling variation in the dimpling process. The current models are developed under the assumption of ideal process performance neglecting process variation. As a result of lack of understanding process variation, the measurement of selected KPI (e.g. dimple height) for given process parameters might violate the given allowance limits and it will lead to erroneous process parameters selection. However, no comprehensive research work has been reported in the laser dimpling process that considers MIMO–based scenario with process variation.

This study is, therefore, focused on development of: *(i)* surrogate model for dimpling process characterization considering multiple–inputs and multiple–outputs (MIMO) system by conducting physical experimentation and using multivariate adaptive regression splines; *(ii)* process capability space (C_p–space) for deterministic and stochastic cases based on the developed surrogate models; and *(iii)* optimization of the process parameters based on the process capability space.

The methodology is developed by introducing the concepts of deterministic and stochastic process capability spaces. The deterministic C_p–space is a measure of the dimpling process capability to satisfy simultaneously all the KPIs allowance limits requirements. Whereas, the stochastic C_p–space is the estimation of process fallout rate which is the probability of making a dimple which satisfies simultaneously all the KPIs limits requirements. The stochastic C_p–space is then used to develop robust dimpling process by identifying process parameters which are less sensitive to the variation in process.

2. Problem Formulation

2.1. Definition of key control characteristics (KCCs) and key performance indicators (KPIs)

The quality performance of a dimple is evaluated by multiple–outputs called in this paper as Key Performance Indicators (*KPIs*), which are delivered by process parameters (multiple–inputs), named in this paper as Key Control Characteristics (*KCCs*). As shown in Fig. 2, the KCCs considered in this study are:

- *Scanning speed* (S_S) – The travelling speed of the laser beam along the upper surface of the workpiece;
- *Focal offset* (F_O) – The distance along the beam axis between the focal point and the interaction of beam and upper surface of the workpiece;
- *Incidence angle* (α) – The angle along the beam movement between the beam axis and the normal vector to the upper surface of the workpiece;
- *Laser track* (L_T) – The linear distance of the beam movement to make a dimple which is parallel to the upper surface of the workpiece.

We observe that the aforementioned KCCs affect not only the selected dimpling process KPIs, but also KPIs of other downstream processes. For example, scanning speed and laser track can affect process cycle time and fixture clamp layout design [37]. Moreover, focal offset and incidence angle can be related to not only dimple height or dimple upper surface area but also they can affect detailed 3D fixture design includes the beam visibility, accessibility and offline programming of the robotic scanner head. This is caused by the fact that the robotic system used to make dimples needs to gain access to the workpiece with no collision between the workpiece/fixture and the laser beam. These examples illustrate the importance analysing dimpling process as MIMO–based system and also to develop methodology which can be expanded to include additional KPIs as required by downstream processes.

Let us define that four KCCs (S_S, F_O, α, L_T) are gathered as in Eq. (1), where i and k represent index of KCC and experimental configuration $\left(KCC_i^{(k)}\right)$; whereas, N_i and N_k are the total number of KCCs and experimental configurations, respectively.

$$\mathbf{KCCs} = \begin{bmatrix} KCC_1^{(1)} & \cdots & KCC_{N_i}^{(1)} \\ \vdots & KCC_i^{(k)} & \vdots \\ KCC_1^{(N_k)} & \cdots & KCC_{N_i}^{(N_k)} \end{bmatrix} \quad (1)$$

The following KPIs are proposed to measure the functionality, strength and aesthetic quality requirements of the dimple which are illustrated in Fig. 2.

- *Dimple Height* (D_H) – This KPI is needed to evaluate the required and predetermined gap between over lapped sheet metal parts which is the main functional objective of a dimple. It is reported in the literature that to make joints with satisfactory quality in laser lap welding dimple height needs to be in the range of [0.1, 0.3] mm [13,33].

- *Dimple upper surface area* (D_U) – This KPI assesses *(i)* strength of the dimple to prevent excessive deformation of the dimple height under compression of clamping force applied during welding process; and, *(ii)* uncertainty as measured by difference between dimple height and the required gap between the faying surfaces during consecutive welding process and caused by geometric surface defects such as roughness, scratches, lines and etc. In essence, the larger dimple upper surface area generates stronger and higher dimples but it creates unwanted surface feature such as dark spots in the lower surface of the workpiece. According to initial screening experiments, we propose dimple upper surface area should be in the range of [1.0, 5.0] mm^2 in order to generate sufficient gap between faying surfaces to achieve satisfactory joint in laser lap welding.
- *Dimple lower surface area* (D_L) – The dark spot appeared in the dimple lower surface is an aesthetic quality requirement which is an unwanted feature in Class-A surfaces in the automotive industry [38]. Thus, the objective is to determine dimple lower surface area which minimizes dimple height variation under compression clamping force in lap joint. According to initial screening experiments, we propose dimple lower surface area should be in the range of [0, 1.5] mm^2.

Let us define three KPIs (D_H, D_U and D_L), as shown in Eq. (2), where j, k and l represent index of KPI, experimental configuration number and its replication $\left(KPI_j^{(k,l)}\right)$; whereas, N_j, N_k and N_l are the total number of KPIs, experimental configurations and replicates, respectively.

$$\mathbf{KPIs} = \left\{ \mathbf{KPI_j} \middle| \forall \mathrm{j}=1,\cdots,N_j \right\}$$
$$\mathbf{KPI_j} = \begin{bmatrix} KPI_j^{(1,1)} & \cdots & KPI_j^{(1,N_l)} \\ \vdots & KPI_j^{(k,l)} & \vdots \\ KPI_j^{(N_k,1)} & \cdots & KPI_j^{(N_k,N_l)} \end{bmatrix} \quad (2)$$

The aforementioned three KPIs are selected as the primary indicators used in this paper to evaluated dimpling process. Additionally, the paper defines lower limits (*LL*) and upper limits (*UL*) for each KCC and KPI, which are given in Tables 1 and 2, respectively.

Table 1 KCCs and their corresponding allowance limits

KCC	Unit	KCC^{LL}	KCC^{UL}
Scanning speed	m/min	2	4
Incidence angle	°	0	20
Laser track	mm	2	4
Focal offset	mm	25	55

The lower and upper limits of all KCCs have been defined by taking into account technological constraints such as maximum scanning speed of the laser beam, minimum laser power intensity on the upper surface of the workpiece to create a dimple. These limits were determined by conducting initial dimpling and welding experiments, results of which are not reported in the paper. The set of all possible KCCs within the allowance limits defines the process parameters space (KCC–space). On the other hand, the lower and upper allowance limits of all KPIs are determined based on aforementioned quality requirements.

Table 2 KPIs and their corresponding allowance limits

KPI	Unit	KPI^{LL}	KPI^{UL}
Dimple height	mm	0.1	0.3
Dimple upper surface area	mm^2	1.0	5.0
Dimple lower surface area	mm^2	0.0	1.5

2.2. Formulation of surrogate modelling for the dimpling process characterization

The proposed modelling approach addresses two key limitations of the currently available models for dimpling process characterization as discussed in the introduction section by taking into consideration; *(i)* approximation of a comprehensive multivariate relations between multiple– inputs (KCCs) and multiple–outputs (KPIs) of the dimpling process, and (ii) process variation over the KCC–space which can be either homoscedasticity (all KPIs across the KCC–space have the same variance) or heteroscedasticity (variability of a KPI is unequal across the KCC–space). The process capability space (C_p–space) is presented to address both limitations by defining a set of KPIs comprehensively evaluate dimpling process and identifying process parameters inside the KCC–space that satisfy the given quality requirements.

Two different scenarios are considered: deterministic and stochastic. In the deterministic scenario, one or many measurements of the KPIs are conducted. Then, the mean values are calculated to compute deterministic surrogate model which estimates the KPI values over the KCC–space. A success rate (binary function) is therefore calculated which determines whether the estimated value is within its lower and upper allowance limits for a given KPI. In case of success, the given process parameters (KCCs) are said to be feasible. However, this modelling approach has its own limitations. Indeed, due the stochastic nature of the KPI measurements, some individual measurements might violate the limits contrary to its estimated value which does not and vice-versa as highlighted in Fig. 3a.

Thus, stochastic scenario is proposed to take into account the mean and variance to calculate the SR which is directly computed from the measured KPI values. Therefore, the effect of

variation can be represented as in the form of the success rate function. Initially, the probability density function is developed either normal or non-normal distribution, using the measured KPI values. Afterwards, the SR value is calculated which is the probability value of satisfying the allowance limits as illustrated shaded regions in Fig. 3a. Finally, stochastic surrogate model (non-binary function) is developed to calculate the SR values over the KCC–space to determine the feasible KCCs for achieving given success rate (β) as highlighted in Fig. 3b

Furthermore, the success rate is also referred as (1 – process fallout rate) in the manufacturing terminology and note is made that the higher success rate is the lower the process fallout rate. Moreover, the allowance limits for KCCs are determined by the equipment capability; whereas, the specification limits for KCCs are determined to satisfy the allowance limits for KPIs and the natural specification limits are determined to satisfy desirable success rate, which are illustrated in Fig. 3c.

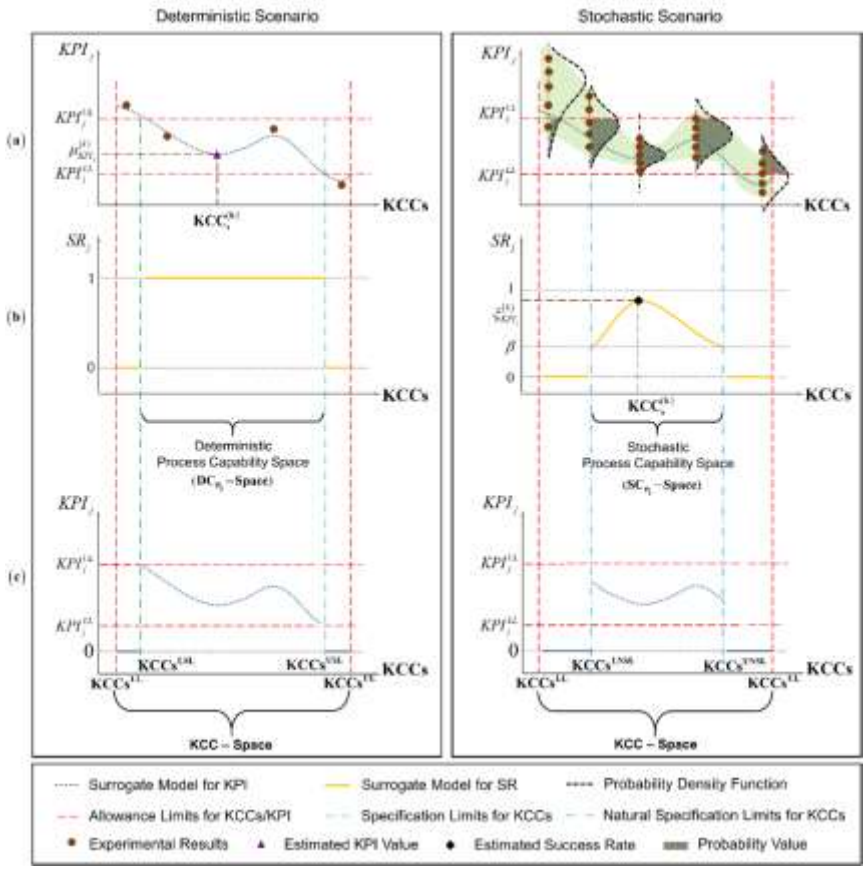

Fig. 3. Conceptual representation deterministic and stochastic scenarios; **(a)** Experimental results **(b)** Success rate models **(c)** Tolerance limits

The observed KPIs might not be independent each other and their joint relationship becomes important to define the PDF function. Therefore, the Pearson correlation coefficient test has been initially conducted to measure dependence among all KPIs, which is defined in Eq. (3).

$$\rho_{mn} = \frac{\mathrm{cov}\left(\mathbf{KPI_m}, \mathbf{KPI_n}\right)}{\sigma_{\mathbf{KPI_m}} \sigma_{\mathbf{KPI_n}}} \qquad \forall m, n = \left\{1, \cdots, N_j\right\} \tag{3}$$

The correlation result $\left(\rho_{ij}\right)$ indicates the linear relationship among KPIs which takes a value between -1 and +1. Even though correlation and dependency are statistically different terms, if KPIs are linearly correlated, it can be deduced that they are dependent each other. As a result, the dependence among KPIs changes the form of the PDF function. The mean value of the k^{th} experimental configuration of the j^{th} KPI is defined in Eq. (4), where $N_s^{(k)}$ is the sample size in the k^{th} experimental configuration.

$$\begin{aligned} \mu_{KPI_j^{(k)}} &= \frac{1}{N_s^{(k)}} \sum_{l=1}^{N_s^{(k)}} KPI_j^{(k,l)} \\ \boldsymbol{\mu}_{\mathbf{KPI_j}} &= \left[\mu_{KPI_j^{(1)}}, \cdots, \mu_{KPI_j^{(k)}}, \cdots, \mu_{KPI_j^{(N_k)}} \right]^{\mathrm{T}} \end{aligned} \tag{4}$$

The PDF function that describes the simultaneous behaviour of the dependent KPIs which is called as "*joint probability density function*" is given in Eq. (5).

$$PDF_{KPI_1^{(k)} \cdots KPI_d^{(k)}} = \frac{1}{\sqrt{(2\pi)^d \left|\sum^{(k)}\right|}} e^{-\frac{1}{2}\left(\mathbf{KPI_d} - \boldsymbol{\mu}_{\mathbf{KPI_d^{(k)}}}\right)^T \left(\sum^{(k)}\right)^{-1} \left(\mathbf{KPI_d} - \boldsymbol{\mu}_{\mathbf{KPI_d^{(k)}}}\right)} \tag{5}$$

where d is the number of the dependent KPIs and it will equal to the number of KPIs $\left(N_j\right)$, if all KPIs are dependent to each other. The symmetric covariance matrix in the k^{th} experimental configuration is given as $\sum^{(k)}$. On the other hand, The PDF function is represented as function of mean value $\left(\mu_{KPI_j^{(k)}}\right)$ and standard deviation $\left(\sigma_{KPI_j^{(k)}}\right)$ for univariate independent KPI, which is given in Eq. (6).

$$PDF_{KPI_j^{(k)}} = \frac{1}{\sqrt{2\pi\sigma_{KPI_j^{(k)}}}} e^{-\frac{1}{2}\frac{\left(KPI_j - \mu_{KPI_j^{(k)}}\right)}{\sigma^2_{KPI_j^{(k)}}}} \tag{6}$$

The Shapiro–Wilk normality test, which provides better results that other normality tests for small sample size [39], is applied to assess the normality assumption for each experimental configuration; and hence, the PDF function is given as a normal distribution. Furthermore, the

number of replication is quite small to directly calculate the standard deviation. Therefore, it is formulated using the range statistics and corrective coefficient (d_2) constant.

The success rate is calculated as a probabilistic approach that is the area under the PDF function. The probability is determined by the integral of the PDF over the given allowance limits, and it is formulated in Eq. (7) for dependent KPIs; whereas, in Eq. (8) for each independent KPI.

$$\xi_{KPI_1^{(k)}\cdots KPI_d^{(k)}} = \int_{KPI_1^{LL}}^{KPI_1^{UL}} \cdots \int_{KPI_d^{LL}}^{KPI_d^{UL}} PDF_{KPI_1^{(k)}\cdots KPI_d^{(k)}}\left(KPI_1^{(k)},\cdots,KPI_d^{(k)}\right) dKPI_1^{(k)}\cdots dKPI_d^{(k)} \qquad \forall k=\{1,\cdots,N_K\} \tag{7}$$

$$\xi_{KPI_j^{(k)}} = \int_{KPI_j^{LL}}^{KPI_j^{UL}} PDF_{KPI_j^{(k)}}\left(KPI_j^{(k)}\right) dKPI_j^{(k)} \qquad \forall j=\{d+1,\cdots,N_J\}, \forall k=\{1,\cdots,N_K\} \tag{8}$$

The general forms of deterministic and stochastic surrogate models for estimating KPI value and the success rate for dependent and independent KPIs are given in Eqs. (9) to (11), respectively.

$$\hat{\mu}_{KPI_j} = \mathbf{F}_{\boldsymbol{\mu}_{\mathbf{KPI_j}}}\left(KCC_1,\cdots,KCC_{N_i}\right) \qquad \forall j=\{1,\cdots,N_j\} \tag{9}$$

$$\hat{\xi}_{KPI_1\cdots KPI_d} = \mathbf{F}_{\xi_{\mathbf{KPI_1\cdots KPI_d}}}\left(KCC_1,\cdots,KCC_{N_i}\right) \tag{10}$$

$$\hat{\xi}_{KPI_j} = \mathbf{F}_{\xi_{\mathbf{KPI_j}}}\left(KCC_1,\cdots,KCC_{N_i}\right) \qquad \forall j=\{d+1,\cdots,N_j\} \tag{11}$$

2.3. Formulation of deterministic and stochastic process capability space

A sub-set of KCC–space is the process capability space (C_p–space), which envelops all the feasible KCCs satisfying the KPIs allowance limits. For the j^{th} KPI, deterministic process capability space $\left(\mathbf{DC_{p_j}}\text{-}\mathbf{Space}\right)$ is expressed in Eq. (12).

$$\mathbf{DC_{p_j}}\text{-}\mathbf{Space}\left(KCC_1,\cdots,KCC_{N_i}\right) = \begin{cases} 1 & if \quad KPI_j^{LL} \le \mathbf{F}_{\boldsymbol{\mu}_{\mathbf{KPI_j}}}\left(KCC_1,\cdots,KCC_{N_i}\right) \le KPI_j^{UL} \\ 0 & otherwise \end{cases} \qquad \forall j=\{1,\cdots,N_j\} \tag{12}$$

The stochastic process capability spaces are defined in Eqs. (13) & (14) for dependent and independent KPIs, respectively.

$$\mathbf{SC_{p_{KPI_1\cdots KPI_d}}}\text{-}\mathbf{Space}\left(KCC_1,\cdots,KCC_{N_i}\right) = \begin{cases} \hat{\xi}_{KPI_1\cdots KPI_d} & if \quad \beta \le \mathbf{F}_{\xi_{\mathbf{KPI_1\cdots KPI_d}}}\left(KCC_1,\cdots,KCC_{N_i}\right) \le 1 \\ 0 & otherwise \end{cases} \tag{13}$$

$$\mathbf{SC_{p_j}}\text{-}\mathbf{Space}\left(KCC_1,\cdots,KCC_{N_i}\right) = \begin{cases} \hat{\xi}_{KPI_j} & if \quad \beta \le \mathbf{F}_{\xi_{\mathbf{KPI_j}}}\left(KCC_1,\cdots,KCC_{N_i}\right) \le 1 \\ 0 & otherwise \end{cases} \qquad \forall j=\{d+1,\cdots,N_J\} \tag{14}$$

where β is the minimal desirable success rate. The identification of the final deterministic and stochastic process capability spaces is done by aggregation individual deterministic and stochastic process capability spaces and obtained from Eq. (15) and Eq. (16), respectively.

$$\mathbf{DC_p - Space} = \bigcap_{j=1}^{N_J} \mathbf{DC_{p_j} - Space} \tag{15}$$

$$\mathbf{SC_p - Space = SC_{p_{KPI_1 \cdots KPI_d}} - Space} \cdot \prod_{j=d+1}^{N_J} \mathbf{SC_{p_j} - Space}. \tag{16}$$

It is noteworthy that d is the number of the dependent KPIs which is determined according to the Pearson correlation coefficient test. The final stochastic process capability space is obtained by the probability theory which is a product of the independent and dependent stochastic process capability spaces. If the all KPIs are dependent, final stochastic process capability is only computed from the dependent stochastic process capability space.

2.4. Process parameter optimization using calculated surrogate models

The aim of this study is to identify optimum KCCs which maximize KPI (evaluated by deterministic surrogate model) and the probability of satisfying the allowance limits of that KPI (evaluated by stochastic surrogate model) at the same time. Therefore, the multi–objective optimization problem can be formally stated in Eq. (17).

$$\begin{aligned} &\text{maximize} && \mathrm{F}_{\mu_{KPI_j}}\left(KCC_1,\cdots,KCC_{N_i}\right), \mathrm{F}_{\xi_{KPI_j}}\left(KCC_1,\cdots,KCC_{N_i}\right), \mathrm{F}_{\xi_{KPI_1\cdots KPI_d}}\left(KCC_1,\cdots,KCC_{N_i}\right) \\ &\text{subject to} && KCC_i^{LL} \le KCC_i \le KCC_i^{UL} \quad \forall i = \{1,\cdots,N_i\} \\ & && KPI_j^{LL} \le \hat{\mu}_{KPI_j} \le KPI_j^{UL} \quad \forall j = \{1,\cdots,N_j\} \end{aligned} \tag{17}$$

3. Generation of the deterministic and the stochastic surrogate models

3.1 Materials

The material used in this study was DX54D hot dip galvanized (GI) steels with nominal zinc coating thicknesses of 20 μm. The chemical composition and mechanical properties of this steel are given in Tables 3 and 4, respectively.

Table 3 Chemical composition DX54D steel (wt %)

Material	Elements (*wt %*)					
	C	Si	Mn	P	S	Ti
DX54D	0.12	0.5	0.6	0.1	0.045	0.3

Two series of experiments were carried out. The first series served to characterise the dimpling process and develop the deterministic and stochastic process capability spaces; dimples were generated on the top surface of zinc coated sheet metal with a thickness of 0.75 mm. The second series was used to validate the calculated optimum KCCs based on the process capability spaces by confirmation experiments which were carried out on coupon experiments.

Table 4 Mechanical properties of steel DX54D

Material	Yield Strength (MPa)	Tensile Strength (MPa)	Total Elongation (%)
DX54D	120 – 220	260 – 350	38

3.2 Experimental setup

Dimpling experiments were carried out using IPG Photonics YLR-4000 laser source with a nominal power of 3 kW at a wavelength of 1064 nm. The laser beam was delivered using an optical fiber of core diameter of 50 μm, projecting the laser beam to a spot of 900 μm diameter. The laser source generates a multi-mode beam with an M^2 of 31.4 (measured by Primes Focus meter) at a central wavelength of 1064 nm. Neither shielding nor backing gases were used during the experiments.

Figure 4 shows the experimental setup for beam quality measurement, laser dimpling and remote welding systems. The laser beam is delivered by COMAU SmartLaser robotic system which is a dedicated system for remote laser welding/dimpling and consists of 4 axes with dynamics and kinematics of a standard industrial robot with an optical system able to deflect the focused beam with high dynamics. The system specifications are given in Table 5.

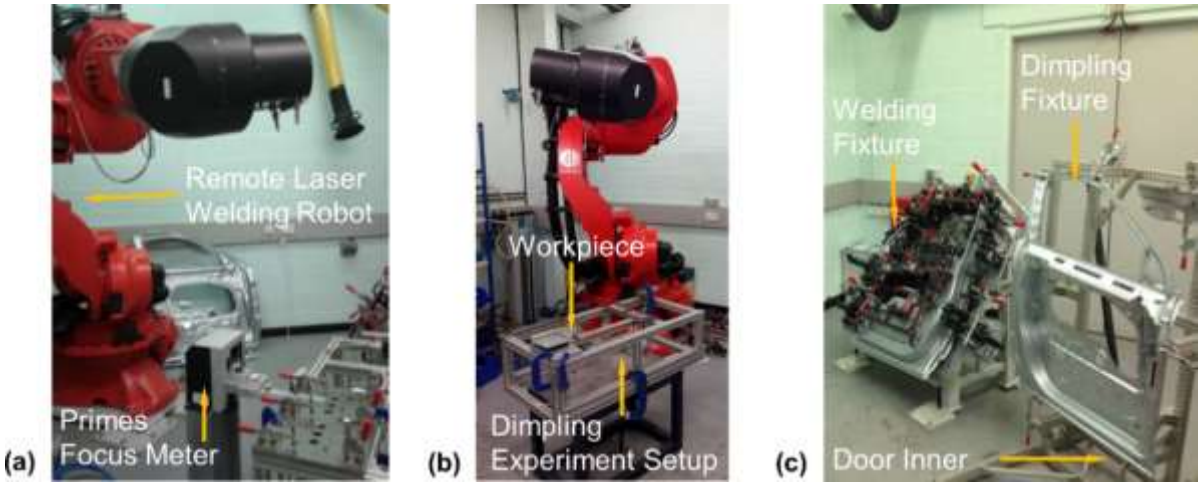

Fig. 4. Overview of the experimental setup **(a)** Beam quality measurement **(b)** Laser Dimpling setup (first series of experiments) **(c)** Remote Laser Welding setup (second series of experiments)

Table 5 Laser focusing and repositioning module (SmartLaser)

Characteristic Feature	Unit	Specification
Collimating length	mm	50
Max focal length	mm	~1200
Measured spot size	μm	900
Working area	mm	700 × 450 × 400
Working distance	mm	min 894 max 1216

3D optical surface profilometer (Bruker, Contour GT) was used to measure dimple height (D_H) and dimple upper spot area (D_U). The top surface of the zinc coated steel was scanned at speed 5μm/s with a vertical resolution of ~10 nm on a rectangle region 4.5 x 6.5 mm. Thus, there are some gaps in the obtained data. The raw data obtained from the optical profilometer was filtered and then reconstructed in 3D which was meshing of the scanned surface area using "*Laplacian smoothing filter*". The experimental setup for profilometer and an example of scanning result with corresponding process parameters are shown in Fig. 5.

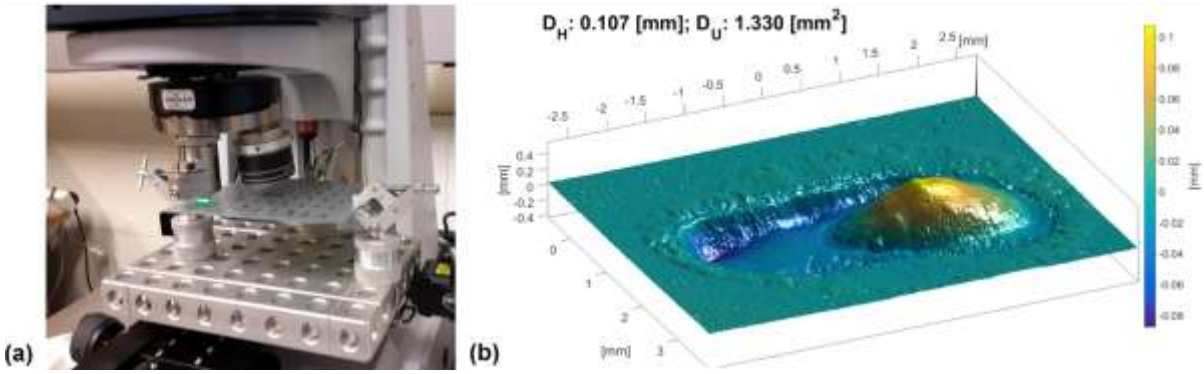

Fig. 5. (a) Experimental setup for profilometer **(b)** An example of 3D reconstruction. Process parameters: S_S: 2 m/min, F_O: 35 mm, α: 20°, L_T: 4 mm

On the other hand, dimple lower surface area (D_L) was computed by image segmentation method using MatLab®. Each image is captured with high resolution camera (3264×2448 pixels), with focal axis perpendicular to the surface of the workpiece to avoid image distortion. Initially, the number of pixel is calculated in 10 mm straight line to obtain scale from pixel length to millimetre; and then, the image was converted into 256 grey levels. After removing the background from the original image, it was binarized (black and white image). The number of black pixels inside the binarized image gives the area in pixel unit. This is converted into millimetre square using the obtain scale to get the corresponding lower surface area (D_L). As an example, the reconstructed D_L measurement is illustrated in Fig. 6.

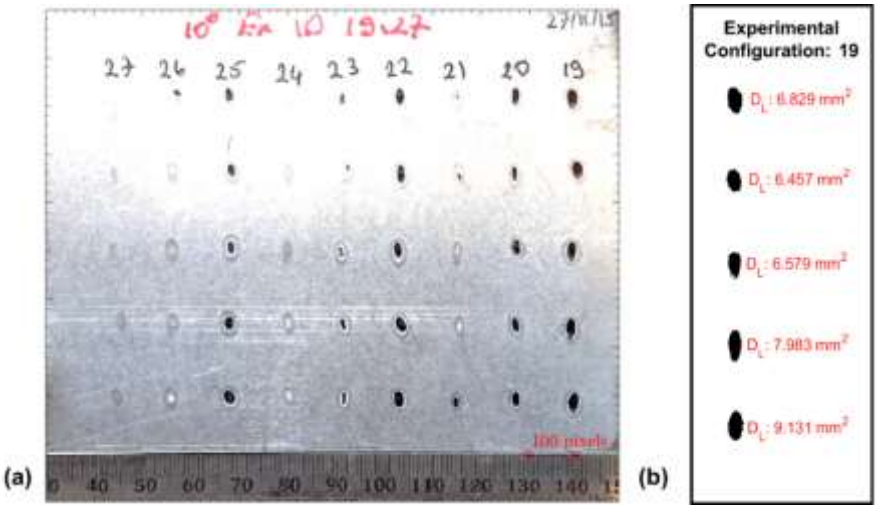

Fig. 6. Measurement of the dimple lower surface area **(a)** Grabbed image with scale bar. **(b)** Dimple lower surface area (D_L) for experiment configuration 19 with 5 replications. Process parameters: S_S: 2 m/min, F_O: 25 mm, α: 10°, L_T: 4 mm

3.3 Design of Experiments

Several methods are available for the design of experiments to establish the relationship between input and output variables, which include, among others, single-factor by single-factor approach, factorial or fractional factorial approaches, Box-Behnken, Doehlet or Taguchi experimental designs. Even though the full factorial design requires larger number of experimental configurations than others alternative techniques, it allows to spread out design point uniformly to obtain complete information on an unknown design function with a limited sample size for capturing both main factors and interactions. Therefore, we adopted a full factorial design approach with 4 – factor and 3 – level requires 81 experimental configurations (N_k) with five replicates resulting 405 experimental runs. The design of experiment table was created in randomize order and it was distributed into 9 batches of sheet metal plates (130 × 110 mm). Thus, each plate had equal number of dimples and dimpling experiments were conducted according to the created DoE table. However, this equal division did not guarantee that each replicate was conducted in different metal plates. Due to the expected non-linear and stochastic nature of the dimpling process, we selected 3 levels for each KCC and the selected experimental levels were shown in Table 6.

Table 6 Key control characteristics and corresponding levels

KCC	Unit	Level [1]	Level [2]	Level [3]
Scanning Speed	m/min	2.0	3.0	4.0
Incidence Angle	°	0.0	10.0	20.0
Focal Offset	mm	25.0	35.0	55.0
Laser Track	mm	2.0	3.0	4.0

Replication is conducted to detect the variation of system. Note is made that the more number of replications is the more accurate estimation of variation within the system. We selected 5 replications because they represent the right balance between expected model accuracy and time needed to perform experiments and collect data (one single dimple experiment, including laser processing, measurement and data collection, took about 2 hours). The paper is intended to provide a general methodological approach, whose accuracy may be enhanced whenever more replications are made available.

3.4 Developing of Surrogate Models

The first objective of this work is to compute a surrogate model capable of analytically formulate relationships between multiple–inputs (KCCs) and multiple–outputs (KPI values and success rates). This study applied multivariable adaptive regression spline (MARS) method developed by Friedman [40]. The MARS method is a non-linear and non-parametric regression that is able to model complex non-linear relationship among input variables by developing regression models locally rather than globally by the dividing the parameter space into several pieces and then performing piecewise fitting in each piece. Furthermore, it does not require larger number of training data sets and long training process compared to other methods such as neural networks, support vector machines [41].

The piecewise fitting is more appropriate for obtained data in dimpling experiments which are actual measurements and calculated success rates. The behaviour of the obtained data in one region inside the KCC–space cannot be easily correlated to its behaviour in other region caused by a sudden change which reduces the goodness of the regression. For instance, high success rate can be achieved in one experimental configuration but low success rate might be obtained in the next experimental configuration. This sudden change can be handle by using piecewise fitting methods.

The MARS models was developed using ARESLab© [42], a dedicated MatLab toolbox. The parameters used for developing the surrogate models were; *(i)* the maximum number of basis functions that included the intercept terms was set as 101. These functions were necessary to build the model in the forward building phase; *(ii)* the maximum degree of interactions between KCCs was set as 4; *(iii)* piecewise cubic type was chosen; *(iv)* the least important basis functions and high-order interactions were eliminated by feature selection and Generalized Cross-Validation (GCV) score in the backward elimination phase and set as 3; and, *(v)* k-fold cross validation (with 20 k-fold) was used for model validation.

4. Development of the deterministic and the stochastic process capability spaces

The second objective of this work is to develop deterministic and stochastic process capability spaces. A probabilistic approach was used to developed the stochastic capability space. In some problems, the measured KPIs might be dependent each other and their simultaneous behaviour defines the probability space. Therefore, the Pearson correlation coefficient test was initially conducted to determine the number of the dependent KPIs (d). As a consequence, a stochastic surrogate model and a stochastic process capability space were computed for the dependent KPIs; whereas, different stochastic surrogate models and stochastics process capability spaces were computed for each independent KPIs.

The Dixon's Q test was employed for identification of outliers for each experimental configuration and KPIs since it was designed for small sample size and assumed normal distribution [43]. When an outlier detected in one of the dependent KPI, the corresponding values in other KPIs were also considered as outlier even if the passed were not identified as outliers. The procedure flow for computing final deterministic and stochastic process capability spaces are summarized in Table 7.

Table 7 The procedure flow for computing process capability spaces

Step	The methodology for computing final process capability spaces
1	Gather measurements for each KPI using Eq. (2)
2	Define number of dependent KPIs using Eq. (3)
3.1	Calculate outliers for each experimental configuration of each KPI using The Dixon's Q test
3.2	Update the number of sample size for each experimental configuration
4.1	Calculate mean for each experimental configuration for each KPI using Eq. (4)
4.2	Calculate standard deviation for each experimental configuration for each KPI $\sigma_{KPI_j^{(k)}} = \frac{\max\left(KPI_j^{(k.l)}\right) - \min\left(KPI_j^{(k.l)}\right)}{d_2}$ $\sigma_{\mathbf{KPI_j}} = \left[\sigma_{KPI_j^{(1)}}, \cdots, \sigma_{KPI_j^{(k)}}, \cdots, \sigma_{KPI_j^{(N_k)}}\right]^{\mathrm{T}} \quad \forall j = \{1, \cdots, N_j\}$
5.1	Calculate PDF for each experimental configuration for dependent KPIs using Eq. (5)
5.2	Calculate PDF for each experimental configuration for each independent KPI using Eq. (6)
6.1	Calculate SR for each experimental configuration for dependent KPIs using Eq. (7)
6.2	Calculate SR for each experimental configuration for each independent KPI using Eq. (8)
7.1	Calculate deterministic surrogate model for each KPI using Eq. (9)
7.2	Calculate stochastic surrogate model for dependent KPIs using Eq. (10)
7.3	Calculate stochastic surrogate model for each independent KPI using Eq. (11)
8.1	Calculate deterministic process capability space for each KPI using Eq. (12)
8.2	Calculate stochastic process capability space for dependent KPIs using Eq. (13)
8.3	Calculate stochastic process capability space for each independent KPI using Eq. (14)
9.1	Calculate final deterministic process capability over KCC–space using Eq. (15)
9.2	Calculate final stochastic process capability over KCC–space using Eq. (16)

5. Process Parameters Optimization

The last objective of this work is optimization of the process parameters based on the deterministic and stochastic process capability spaces. Both deterministic and stochastic C_p–spaces provide necessary models for selection KCCs to optimize the KPIs using various strategies reflecting the engineering needs of the dimpling process. In general, the optimisation entails two competing objectives; *(i)* to obtain maximum KPI value; and, *(ii)* to maximize the probability of satisfying the allowance limits of selected KPI. It is important to note that the requirements for dimpling process are determined by downstream processes such as assembly fixture design and optimization [37]. For example, assembly fixture design for welding which is a downstream process might require a specific KCCs/KPIs configuration which will impose the dimpling process to achieve the best success rate in satisfying the requirements of achieving lower allowance limits of KPIs. Therefore, the proposed optimization strategy is based on ε-constraint method rather than solving Pareto Frontier. This involves optimization of success rate in achieving pre–selected KPIs configuration and using the other functions as constraints.

In this paper, three design options are defined to optimize all KPIs. The first design option maximizes success rate of the dependent KPIs which addresses the functional and strength requirement of a dimple (i.e. D_H, D_U) to control simultaneously minimum gap requirement and strength of dimple. Similarly, the second design option evaluates the success rate of the independent KPI which focuses on aesthetic requirements of a dimple (i.e. D_L) that is important for Class–A surfaces. The other design options are combination of these options and handled as multi–objective optimization. Table 8 describes the proposed optimization strategies for various pre–defined KCCs/KPIs configurations.

Table 8 Proposed options for process parameters selection

Design Option	Objective Function	Constraint Functions		
		Deterministic Constraint	Stochastic Constraint	Bounded Process Parameters
1	$\max \mathbf{F}_{\xi_{\mathbf{KPI_1KPI_2}}}$	$\mathbf{F}_{\mu_{\mathbf{KPI_1}}} \geq KPI_1^{LL}$ $\mathbf{F}_{\mu_{\mathbf{KPI_2}}} \geq KPI_2^{LL}$	-	
2	$\max \mathbf{F}_{\xi_{\mathbf{KPI_3}}}$	$\mathbf{F}_{\mu_{\mathbf{KPI_3}}} = KPI_3^{LL}$	-	$KCC_i^{LL} \leq KCC_i \leq KCC_i^{UL}$ $\forall i = \{1, \cdots, N_i\}$
3	$\max \mathbf{F}_{\xi_{\mathbf{KPI_1KPI_2}}}$	$\mathbf{F}_{\mu_{\mathbf{KPI_1}}} \geq KPI_1^{LL}$ $\mathbf{F}_{\mu_{\mathbf{KPI_2}}} \geq KPI_2^{LL}$ $\mathbf{F}_{\mu_{\mathbf{KPI_3}}} = KPI_3^{LL}$	$\mathbf{F}_{\xi_{\mathbf{KPI_3}}} \geq \beta$	

6. Results and discussions

6.1 Statistical data analysis

The total number of KCCs, KPIs, experimental configurations, replication and dependent KPIs are determined as N_i, N_j, N_k, N_l and d, respectively. The dependency among KPIs are evaluated using the Pearson product-moment correlation coefficient test and its result (ρ) takes a value between +1 and −1, where 1 is total positive linear correlation, 0 is no linear correlation, and −1 is total negative linear correlation. The result of the Pearson test is given in Eq. (18). According to results, dimple height (D_H) and dimple upper surface area (D_U) are chosen as dependent KPIs and dimple lower surface area (D_L) is independent from other KPIs.

$$\rho_{mn} = \frac{\mathrm{cov}\left(\mathbf{KPI_m}, \mathbf{KPI_n}\right)}{\sigma_{\mathbf{KPI_m}} \sigma_{\mathbf{KPI_n}}} \quad \forall m, n = \{1, \cdots, 3\}$$
$$= \begin{bmatrix} 1 & 0.7852 & 0.2409 \\ 0.7852 & 1 & 0.5515 \\ 0.2409 & 0.5515 & 1 \end{bmatrix} \tag{18}$$

The goodness of surrogate models is assessed by computing the determination of coefficient (R^2) and root mean square error (RMSE) and the MARS models are compared with second and third order polynomial regressions which are reported in

Table **9**. The success rate in the stochastic case is not a binary value and it gets any value between zero and one. However, its behaviour in one region inside the KCC–space cannot be easily correlated to its behaviour in other region. This change can be handle by using piecewise fitting methods and better R^2 and RMSE are obtained in MARS model. The obtained MARS models and the measured KPIs are given in the in the Appendix.

Table 9 R^2 & RSME values for different surrogate models

Surrogate Model	MARS		2nd order polynomial		3rd order polynomial	
	R^2	RSME	R^2	RSME	R^2	RSME
$\mathbf{F}_{\mu_{KPI_1}}$	0.9281	0.0117	0.9527	0.0266	0.9624	0.0235
$\mathbf{F}_{\mu_{KPI_2}}$	0.9634	0.1219	0.9293	0.3288	0.9358	0.3025
$\mathbf{F}_{\mu_{KPI_3}}$	0.9874	0.2213	0.9506	0.5621	0.9534	0.5329
$\mathbf{F}_{\xi_{KPI_1 KPI_2}}$	0.8872	0.1450	0.8068	0.2766	0.8114	0.1866
$\mathbf{F}_{\xi_{KPI_3}}$	0.9754	0.0684	0.9187	0.2241	0.9039	0.1353

6.2 Deterministic Surrogate Models

In the deterministic scenario, the mean values are calculated to compute surrogate model which estimates the KPI values over the KCC–space. The results of these deterministic surrogate models are illustrated in Figs. 7 to 9 for varying scanning speed (S_S) and incidence angle (α) for constant laser track (L_T) and focal offset (F_O) values. These figures provide two types of information; *(i)* the effect of the process parameters on KPIs which can be directly used by the automotive industry; and, *(ii)* individual deterministic process capability spaces $\left(\mathbf{DC_{p_j}\text{-}Space}\right)$ which lead to final deterministic process capability space $\left(\mathbf{DC_{p}\text{-}Space}\right)$. It is interesting to note that dimple is formed in the same direction with laser track movement for higher defocus (~5 mm) whereas dimple is formed in the opposite direction of the laser movement for lower focal offset (~25mm). This behaviour is one of the findings of this study and is shown in Fig. 10. It can be explained by the fact that larger defocusing generates bigger laser beam spot size which leads to a drop in power intensity. In this case the molten material is moved forward by the movement of the laser beam. The dimples obtained in this condition are characterized by a cavity in the rear and higher dimple in front, which is highlighted in Fig. 2.

6.2.1 Characterization of dimple height (D_H)

According to the literature, dimple height decreases with scanning speed. However, as predicted in Fig. 7, this can only be obtained for high focal offset (~55 mm) and constant incidence angle. For low focal offset (~25 mm), the laser track clearly affects the dimple height, whilst a bipolarized pattern can be observed because of the mutual interaction between speed and incidence angle. At medium focal offset (~35), scanning speed slightly affects dimple height, whilst the interaction between laser track and incidence angle generates a unipolar pattern. The highest dimple height is observed around 5 – 10 degrees. The reason for this could be the amount of energy absorbed by the material and tilted keyhole that pushes the melting upwards. It can be deduced that the dimple height increases while increasing laser track as also indicated in the literature [27].

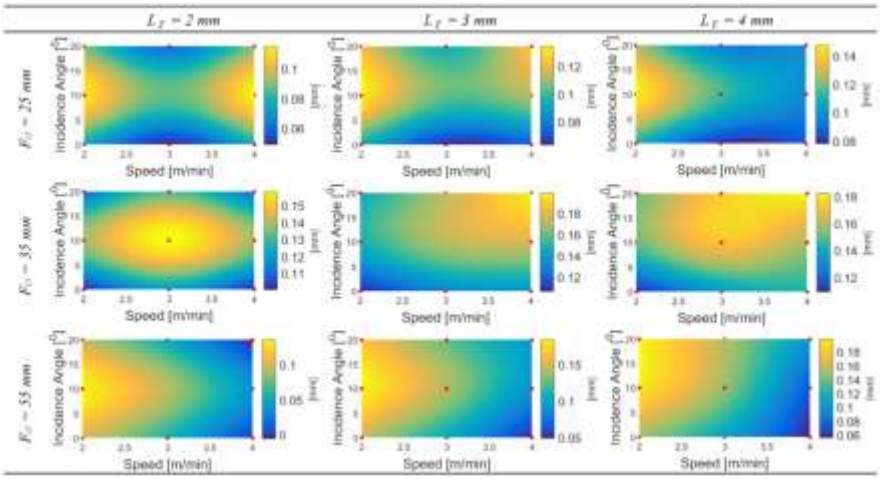

Fig. 7. The estimated dimple height value (D_H) over KCC–space in the deterministic scenario

6.2.2. Characterization of dimple upper surface area (D_U)

Dimple upper surface area (D_U) decreases with increasing scanning speed whist other parameters are kept constant. However, it increases with increasing both scanning speed and laser track but decreases with increasing both scanning speed and focal offset. It is evident that increasing laser track results in higher and larger dimple since the longer displacement creates longer trailing jet on the surface as also indicated in the literature [24]. The correlation patterns exhibit a unipolar shape, which tends to be elongated moving toward higher laser track and focal offset.

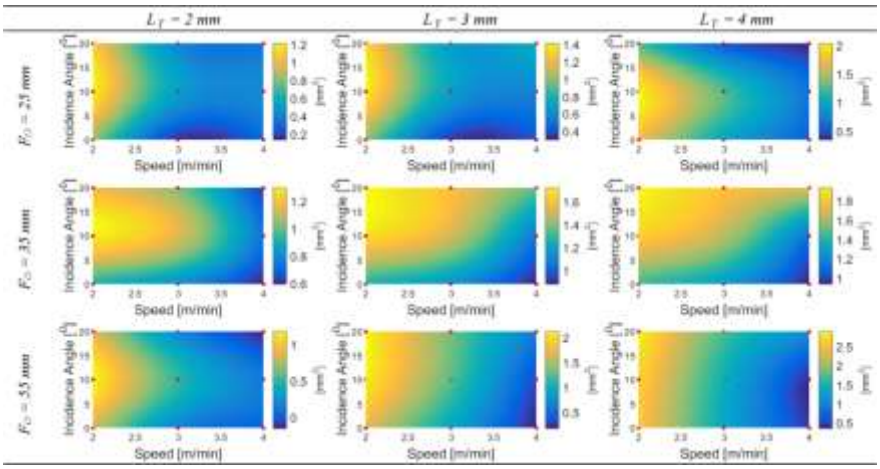

Fig. 8. The estimated dimple upper surface value (D_U) over KCC–space in the deterministic scenario

6.2.3. Characterization of dimple lower surface area (D_L)

It is interesting to note that the main and interaction effects of incidence angle into dimple lower surface area (D_L) can be negligible and it can be seen in Fig. 9 that the correlation pattern is almost identical. On the other hand, D_L is directly correlated with laser track and inversely

correlated with focal offset and scanning speed. The minimum D_L is observable for medium (~35 mm) and high (~55 mm) focal offset and lower laser track (~ 2 mm).

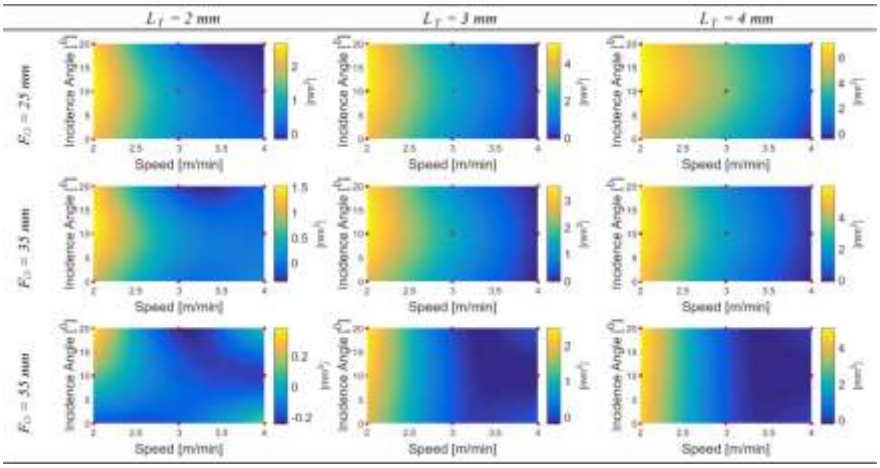

565 **Fig. 9.** The estimated dimple lower surface value (D_L) over KCC–space in the deterministic scenario

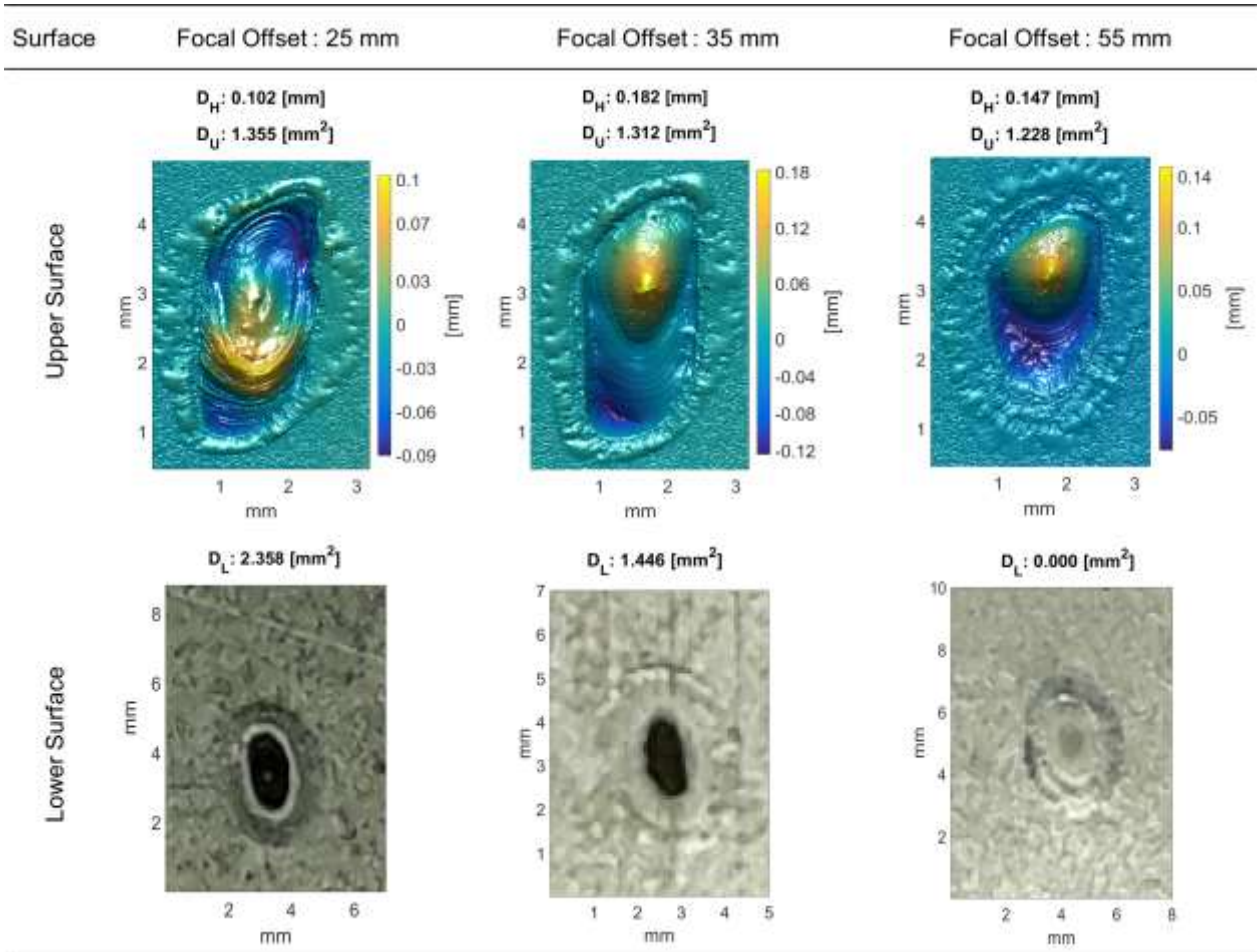

Fig. 10. Effect of focal offset on three KPIs when process parameters are constant at S_S: 3 m/min, α: 10°, L_T: 3 mm. (Upper Surface) Surface profilometer results – (Lower Surface) Image processing results

570

*6.3 Deterministic Process Capability Space (**DC_P – Space**)*

The deterministic process capability space (**DC_P – Space**) is illustrated in Fig. 11. The shaded area represents the feasible region and any value inside corresponds to feasible process parameters (KCCs) which simultaneously satisfy all quality requirements defined in Table 2. According to the **DC_P – Space** result, feasible process parameters cannot be achieved for lower focal offset (~25 mm) since dimple lower surface area (D_L) is more likely to exceed its allowance limits that is highlighted in Fig. 9. The reason might be lower focal offset creates higher power intensity and thus more amount of material is molten which results in wider and deeper molten pool. The rate of change of the laser intensity determines the physical phenomena between material and laser beam. For instance, slow speed, short laser track and low focal offset result higher energy intensity rate and thus, higher dimple but larger dimple lower surface area is occurred. Therefore, feasible regions are gathered in the medium level of the process parameters.

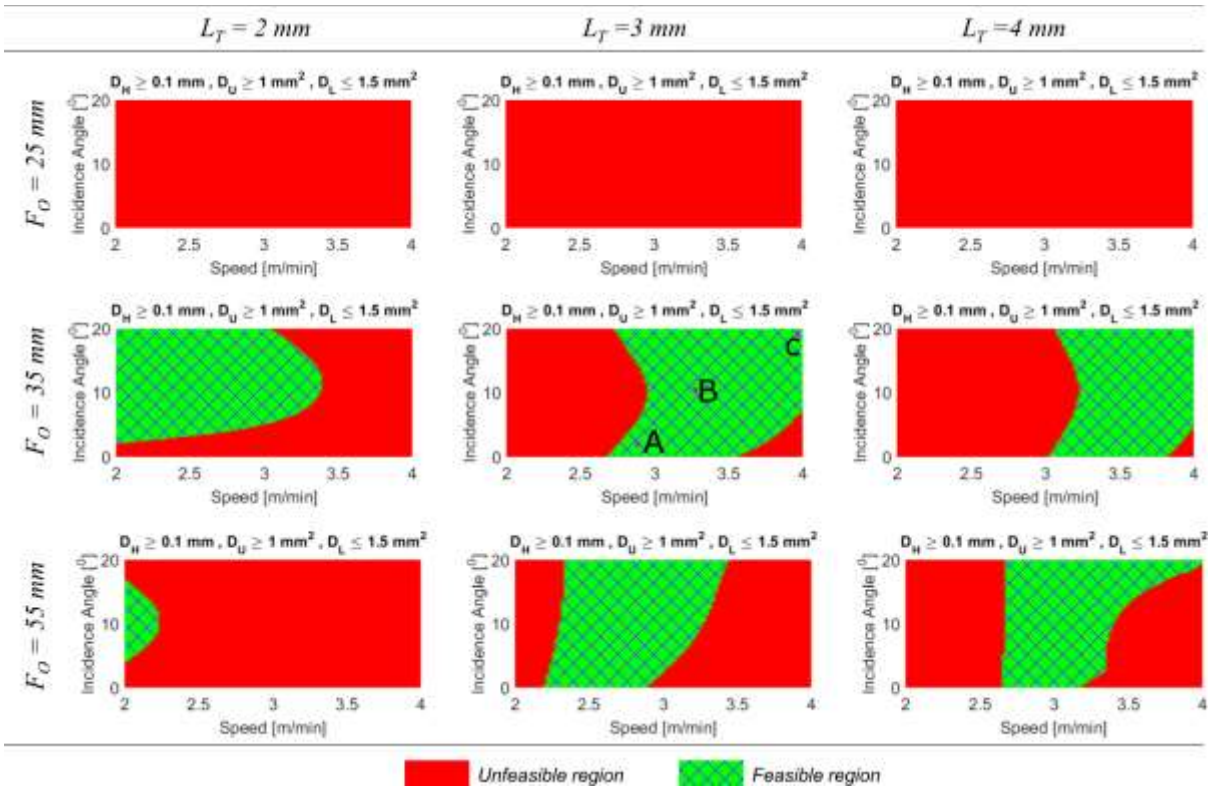

Fig. 11. Deterministic Process Capability Space (**DC_P – Space**) for laser dimpling process

*6.4 Stochastic Process Capability Space (**SC_P – Space**)*

The calculated stochastic process capability space (**SC_P–Space)** is presented in Fig. 12 It represents the simultaneous product of the stochastic process capability spaces defined in Eq. (16). The achievable success rates of the dimpling process are displayed in contour plot by

initially selecting minimal desirable success rate (β) at zero in Fig. 12. Therefore, it will provide more information to select a set of KCCs. For example, point **A** and **B** are inside the feasible region in Fig. 11 which define two different sets of KCCs that simultaneously satisfy KPIs allowance limits. On the contrary, these points represented in Fig. 12 are different success rates since the process variation is less at the point **B.** Therefore, point **B** provide more robust process parameters (KCCs) and **SC_P–Space** can be utilized to select KCCs according to pre–defined success rate (β). Furthermore, the deterministic process capability space and stochastic process capability space have to follow same pattern since probability value is a function of mean and variation.

According to results, higher success rate regions are concentrated at the medium focal offset (~35 mm). The success rate is nearly zero at lower focal offset (~25 mm) thus confirming the results obtained by the **DC_P–Space** model. According to the results, the minimal desirable success rate (β) was set at 0.8 and it was highlighted in shaded region in Fig. 12.

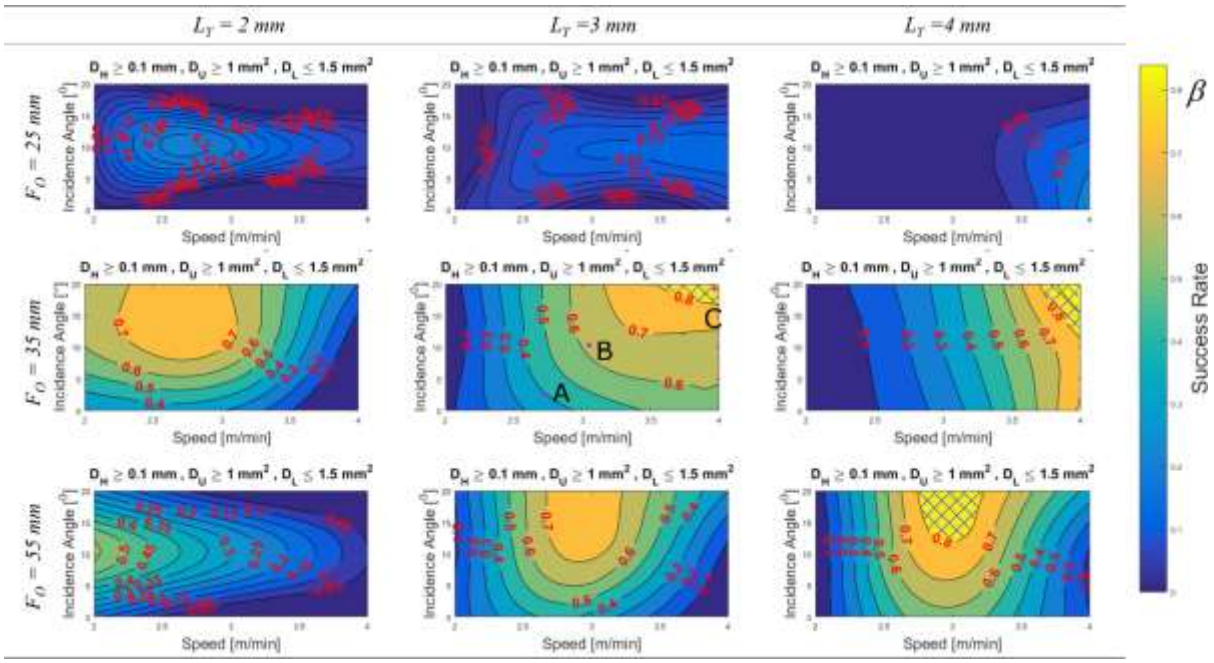

Fig. 12. Stochastic Process Capability Space (**SC_P – Space**) for laser dimpling process

6.5 Process parameters selection and optimisation

Despite the fact that evolutionary algorithms do not guarantee the global optimum, their convergence speeds to the optimal results (nearly global) are better than those of the traditional techniques. Thus, evolutionary algorithms have been used for optimization of real-world problems in many applications instead of traditional techniques [44–47]. Therefore, genetic algorithm was implemented to solve the process parameter selection and optimization problem.

Population size, probability of crossover and mutation numbers were selected as 500, 0.60 and 0.12, respectively.

In this paper, we define three design options to optimize all KPIs which are described in Table 8 and the optimization results are given in Table 10. The results indicate that the optimum configurations are concentrated between medium (~35 mm) and high (~55 mm) focal offset and higher laser track (~4 mm) and medium scanning speed (~3 mm). This can be explained by the amount of time spent by the laser power intensity on the workpiece. It can be deduced that by decreasing interaction time less amount of materials was molten and molten pool becomes shallow because less amount of laser energy was absorbed. The design option three is approximately illustrated as Point **C** in Figs. 11 and 12.

Table 10 Optimization results

Design Option	S_S	α	L_T	F_O	$\hat{\mu}_{KPI_1}$	$\hat{\mu}_{KPI_2}$	$\hat{\mu}_{KPI_3}$	$\hat{\xi}_{KPI_1 \cdots KPI_2}$	$\hat{\xi}_{KPI_3}$
1	2.0020	15.0069	3.9692	54.9941	0.198	2.756	4.868	1.000	0.000
2	3.3709	0.2704	3.0229	52.8982	0.092	0.710	0.000	0.283	1.000
3	3.9967	19.9778	3.4845	37.2153	0.199	1.592	0.000	1.000	0.993

In order to validate the optimization results obtained in Table 10 and estimated values from the surrogate models defined in Eqs. (9), to (11), confirmation experiments were carried out by coupon experiments. Five replications of each design option were performed on a 10 x 40 mm sheet metal with a thickness of 0.75 mm and the results are reported in Table 11. It shows measured 5 replications for each KPI and their mean and success rate. These values are computed according to the methodological flow from Step 1 to Step 6.2 which are presented in Table 7. These calculated values are compared against estimated values from the developed surrogate models.

Table 11 Validation of the optimization results for all design options

Design Option	KPI	Rep. 1	Rep. 2	Rep. 3	Rep. 4	Rep. 5	$\mu_{KPI_\bullet}$	$\hat{\mu}_{KPI_\bullet}$	$\xi_{KPI_\bullet}$	$\hat{\xi}_{KPI_\bullet}$
1	D_H	0.183	0.190	0.185	0.209	0.189	0.1912	0.198	1	1
	D_U	2.184	2.055	2.080	2.192	2.154	2.133	2.756	1	1
	D_L	4.467	4.318	4.415	5.028	3.417	4.329	4.868	0	0
2	D_H	0.124	0.13	0.114	0.084	0.118	0.114	0.092	0.588	0.283
	D_U	1.123	1.186	1.037	0.776	1.076	1.0396	0.710	0.588	0.283
	D_L	0.000	0.000	0.000	0.000	0.000	0.000	0.000	1	1
3	D_H	0.207	0.198	0.184	0.179	0.179	0.1894	0.199	0.996	1
	D_U	1.741	1.707	1.647	1.261	1.438	1.513	1.592	0.996	1
	D_L	0.000	0.000	0.000	0.000	0.000	0.000	0.000	1	0.993

These design options are offered to find robust process parameters to obtain maximum dimple height and upper surface; and, minimum dimple lower surface area. The first option studies maximizing mean and success rate of dimple height and upper surface area without considering the dimple lower surface. According to the results, the calculated and estimated mean and success rates are quite similar. However, this similarity is not achieved for the second design option. The second option considers only to obtain robust parameters for minimum dimple lower surface area. The variation of the D_H and D_U at this point are more than measured values and dimple upper surface might be also correlated with dimple lower surface area. These reasons might cause the different in the calculated and estimated values.

The laser dimpling process is currently utilized for the laser lap welding of zinc coated steels, especially automotive industry. The dimples generate a small gap between faying surfaces where the zinc vapour is vented out through. However, obtaining a constant gap without having a darker spot at the back side of the steel are the major challenges of the process. An optimum set of process parameter was validated by welding experiments and results are given in Fig. 13. The figure shows images of welded specimen before and after the optimization of laser dimpling process. The dark spots are not visible on the lower surface and there are no spatters around the stitch after implementing optimum laser dimpling process parameters. Likewise, the quality of weld seam is improved, no blow holes are detected in the weld seam.

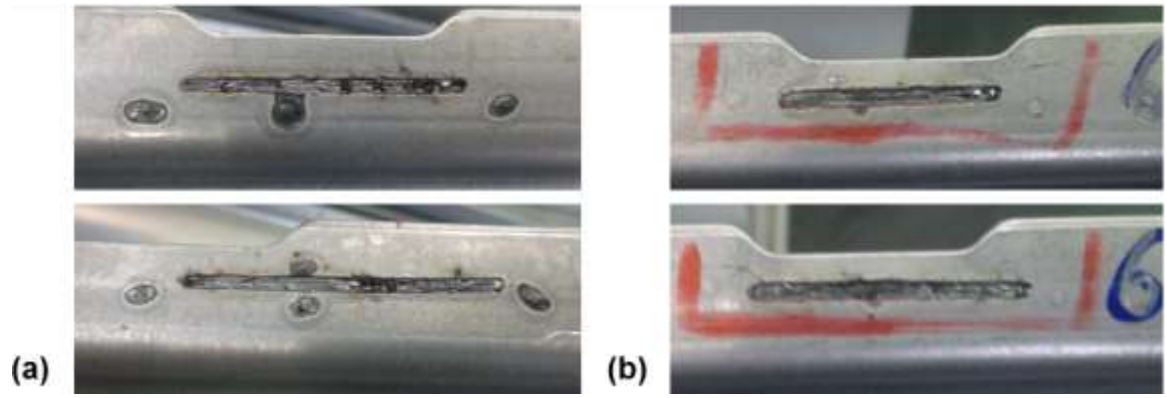

Fig. 13 Remote laser welded joint. (**a**) – Trial and error approach before optimization. (**b**) – Optimized configuration based on the proposed methodology

7 Conclusions and Final Remarks

This paper presents a novel methodology to select process parameters for laser dimpling process. It is based on the process capability space which allows the estimation of a desired process fallout rate in the case of quality failures or violation of process requirements. The success rate is offered to measure the process fallout rate using probabilistic approach. First,

two surrogate models are developed to estimate mean and success rate over the defined process parameters space; and then, the process capability space is computed using the developed surrogate models. Finally, the optimize the mean and success rate based on the minimal desirable success rate (β) using multi-objective optimization methods to reduce variation in the process and to find the robust parameters. Furthermore, the process mean is illustrated in deterministic process capability space (**DC_p–Space)**; whereas, success rate, indirectly process variation, is in stochastic process capability space (**SC_p–Space**). It is noteworthy that optimization the process variation does not guarantee maximizing the mean value. Thus the optimization problem is considered as multi-objective optimization with two competing objectives.

The industrial needs are also addressed in the paper and two new key performance indicators (D_U, D_L) which are first time offered in this paper. The D_U is required to control the gap between faying surfaces, whereas the D_L affects post weld operations. For example, a large D_L (a dark black spot) is unwanted for the downstream process such as it requires additional process to cover these dark spots. Furthermore, four process parameters (S_S, α, L_T, F_O) are offered to have a more comprehensive characterization of the process and to determine their effect on the proposed KPIs. These parameters are selected because scanning speed and laser track can affect the process cycle time and focal offset and incidence angle can be related to the beam visibility, accessibility and offline programming of the robot scanner head.

The following guidelines have been pointed out: for lower focal offset, dimples are formed in the opposite direction of the laser beam movement; whereas, they generate in the same direction for larger defocus (~55 mm). In addition to that, larger defocus will lead to a reduction in the dimple lower surface area. Conversely, increasing laser track will result in a reduction of the dimple lower surface area. It can be concluded that power intensity and the rate of change of the power intensity are the key factors affecting the formation of the laser dimple.

The current best practice for process parameters selection is based on costly and time consuming trial and error approaches (up to 2-3 weeks to setup the proper combination of process parameter for door assembly systems). The proposed methodology offers the following opportunity and applicability: (*i*) selection and optimization of process parameters at early design stage; (*ii*) identification of risky areas and low reliable parameters settings which help to speed-up the process of detecting and correcting defects. This will lead to shorten the time for design and commissioning and reduce production scraps.

The disadvantages of this approach can be summarized as follow: (*i*) the required number of replication to calculate a smooth PDF function to compute success rate. This number can be determined by an initial screen experiments with high number of replication. (*ii*) deterministic and stochastic surrogate models are developed based on the process parameters which can be easily controllable without neglecting the noise variables and their interaction with process parameters. However, this can be handled by accurately designing experiment.

The proposed methodology offers a unique simulation tool which is generic and can be applied not only to laser dimpling process but can also be exploited in the context of selection and optimization of process parameters with heteroscedasticity. This research will be further expanded to integrate the developed surrogate models with task planning and sequencing algorithms in order to simultaneously optimize quality, cost and cycle time of robotic remote laser welding systems.

Acknowledgements

This study was partially supported by the EU research project EU-FP7 FoF-ICT-2011.7.4: RLW Navigator, by the UK EPSRC project EP/K019368/1: Self-Resilient Reconfigurable Assembly Systems with In-process Quality Improvement and by the Republic of Turkey Ministry of National Education Post-Graduate Scholarship.

References

[1] D. Ceglarek, M. Colledani, J. Vanca, D.Y. Kim, C. Marine, M. Kogel-Hollacher, A. Mistry, L. Bolognese, Rapid deployment of remote laser welding processes in automotive assembly systems, CIRP Ann. - Manuf. Technol. 64 (2015) 389–394. doi:10.1016/j.cirp.2015.04.119.

[2] S. Hörnström, J. Karlsson, W.J. Van Ooij, N. Tang, H. Klang, Paint adhesion and corrosion performance of chromium-free pretreatments of 55% Al-Zn-coated steel, J. Adhes. Sci. Technol. 10 (1996) 883–904. doi:http://dx.doi.org/10.1163/156856196X00913.

[3] A. Ribolla, G.L. Damoulis, G.F. Batalha, The use of Nd:YAG laser weld for large scale volume assembly of automotive body in white, J. Mater. Process. Technol. 164–165 (2005) 1120–1127. doi:10.1016/j.jmatprotec.2005.02.104.

[4] Y. Kawahito, M. Mizutani, S. Katayama, S. Steel, Investigation of high-power fiber laser welding phenomena of stainless steel, Trans. JWRI. 36 (2007) 11–16.

[5] A.K. Sinha, D.Y. Kim, D. Ceglarek, Correlation analysis of the variation of weld seam and tensile strength in laser welding of galvanized steel, Opt. Lasers Eng. 51 (2013) 1143–1152. doi:10.1016/j.optlaseng.2013.04.012.

[6] P. Norman, J. Karlsson, A.F.H. Kaplan, Monitoring undercut , blowouts and root sagging during laser beam welding, 5th Int. WLT-Conference Lasers Manuf. (2009) 355.

[7] G. Chen, L. Mei, M. Zhang, Y. Zhang, Z. Wang, Research on key influence factors of laser overlap welding of automobile body galvanized steel, Opt. Laser Technol. 45 (2013) 726–733. doi:10.1016/j.optlastec.2012.05.002.

[8] R. Fabbro, F. Coste, D. Goebels, M. Kielwasser, Study of CW Nd-Yag laser welding of Zn-coated steel sheets, J. Appl. Phys. D. (2006) 401–409. doi:10.1088/0022-3727/39/2/024.

[9] Y. Pan, I.M. Richardson, Keyhole behaviour during laser welding of zinc-coated steel, J. Phys. D. Appl. Phys. 44 (2011) 45502. doi:10.1088/0022-3727/44/4/045502.

[10] F. Briand, K. Chouf, P. Lefebvre, Method and installation for laser welding with a N2/He gas mixture, the N2/He content being controlled according to the laser power, 7385158B2, 2008.

[11] S. Yang, B. Carlson, R. Kovacevic, Laser Welding of High-Strength Galvanized Steels in a Gap-Free Lap Joint Configuration under Different Shielding Conditions, Weld. J. 90 (2011) 8–18.

[12] W. Chen, P. Ackerson, P. Molian, CO2 laser welding of galvanized steel sheets using vent holes, Mater. Des. 30 (2009) 245–251. doi:10.1016/j.matdes.2008.05.009.

[13] R. Akhter, W.M. Steen, K.G. Watkins, Welding Zinc-Coated Steel with a Laser and the Properties of the Weldment, J. Laser Appl. 3 (1991) 9. doi:10.2351/1.4745277.

[14] D.C. Weckman, H.W. Kerr, D.M. Hirak, Nd : YAG Laser Beam Welding of Coated Steels Using a Modified Lap Joint Geometry, Weld. J. (1996) 162–170.

[15] T.J. Jokinen, A.S. Hovikorpi, V. Kujanpaa, Effect of an air gap on the properties of high power Nd: YAG laser welds, in: ICALEO'98- Int. Congr. Appl. Laser Electro-Optics, Orlando, US, 1998: pp. 103–112.Ri

[16] Z. Chen, S. Yang, C. Wang, X. Hu, X. Shao, J. Wang, A study of fiber laser welding of galvanized steel using a suction method, J. Mater. Process. Technol. 214 (2014) 1456–1465. doi:10.1016/j.jmatprotec.2014.02.013.

[17] X. Li, S. Lawson, Y. Zhou, F. Goodwin, G. F., Novel technique for laser lap welding of zinc coated sheet steels, J. Laser Appl. 19 (2007) 259. doi:10.2351/1.2795755.

[18] A.K. Dasgupta, J. Mazumder, Laser welding of zinc coated steel: an alternative to resistance spot welding, Sci. Technol. Weld. Join. 13 (2008) 289–293.

[19] S. Iqbal, M.M.S. Gualini, F. Grassi, Laser welding of zinc-coated steel with tandem beams: Analysis and comparison, J. Mater. Process. Technol. 184 (2007) 12–18. doi:10.1016/j.jmatprotec.2006.10.043.

[20] M.R. Kronthaler, S. Braunreuther, M.F. Zaeh, Bifocal hybrid laser welding- More than a superposition of two processes, Phys. Procedia. 12 (2011) 208–214. doi:10.1016/j.phpro.2011.03.027.

[21] J. Ma, F. Kong, B. Carlson, R. Kovacevic, Two-pass laser welding of galvanized high-strength dual-phase steel for a zero-gap lap joint configuration, J. Mater. Process. Technol. 213 (2013) 495–507. doi:10.1016/j.jmatprotec.2012.10.019.

[22] J. Zhou, H.L. Tsai, T.F. Lehnhoff, Investigation of transport phenomena and defect formation in pulsed laser keyhole welding of zinc-coated steels, J. Phys. D. Appl. Phys. 39 (2006) 5338–5355. doi:10.1088/0022-3727/39/24/036.

[23] Y.F. Tzeng, T. Yih-Fong, Gap-free lap welding of zinc-coated steel using pulsed CO2 laser, Int. J. Adv. Manuf. Technol. 29 (2006) 287–295. doi:10.1007/s00170-005-2522-3.

[24] J. Blackburn, P. Hilton, Producing surface features with a 200 W Yb-fibre laser and the Surfi-Sculpt process, Phys. Procedia. 12 (2011) 529–536. doi:10.1016/j.phpro.2011.03.065.

[25] C. Earl, P. Hilton, B. O'Neill, Parameter Influence on Surfi-Sculpt Processing Efficiency, Phys. Procedia. 39 (2012) 327–335. doi:10.1016/j.phpro.2012.10.045.

[26] H. Gu, Laser lap welding of zinc coated steel sheet with laser-dimple technology, J. Laser Appl. 22 (2010) 87. doi:10.2351/1.3485596.

[27] H. Gu, B. Shulkin, A practical use of humping effect in laser beam welding, J. Laser Appl. 23 (2011) 12001. doi:10.2351/1.3538988.

[28] M.H. Cho, D.F. Farson, Understanding Bead Hump Formation in Gas Metal Arc Welding Using a

Numerical Simulation, Metall. Mater. Trans. B. 38 (2007) 305–319. doi:10.1007/s11663-007-9034-5.

[29] C.S. Wu, Z.K. Hu, Y.M. Zhang, Suppression of weld-bead defects and increase in the critical welding speed during high-speed arc welding, Proc. Inst. Mech. Eng. Part B J. Eng. Manuf. 223 (2009) 751–757. doi:10.1243/09544054JEM1369SC.

[30] P. Berger, H. Hügel, A. Hess, R. Weber, T. Graf, Understanding of humping based on conservation of volume flow, Phys. Procedia. 12 (2011) 232–240. doi:10.1016/j.phpro.2011.03.030.

[31] T. Ilar, I. Eriksson, J. Powell, A. Kaplan, Root Humping in Laser Welding – an Investigation based on High Speed Imaging, Phys. Procedia. 39 (2012) 27–32. doi:10.1016/j.phpro.2012.10.010.

[32] C. Thomy, T. Seefeld, F. Vollertsen, Humping Effect in Welding of Steel with Single-Mode Fibre Laser, Weld. World. 52 (2013) 9–18. doi:10.1007/BF03266636.

[33] D. Colombo, B. Previtali, Laser dimpling and remote welding of zinc-coated steels for automotive applications, Int. J. Adv. Manuf. Technol. 72 (2014) 653–663. doi:10.1007/s00170-014-5690-1.

[34] W. Huang, R. Kovacevic, A neural network and multiple regression method for the characterization of the depth of weld penetration in laser welding based on acoustic signatures, J. Intell. Manuf. 22 (2011) 131–143. doi:10.1007/s10845-009-0267-9.

[35] U. Reisgen, M. Schleser, O. Mokrov, E. Ahmed, Statistical modeling of laser welding of DP/TRIP steel sheets, Opt. Laser Technol. 44 (2012) 92–101. doi:10.1016/j.optlastec.2011.05.025.

[36] Q. Shi, D. Gu, M. Xia, S. Cao, T. Rong, Effects of laser processing parameters on thermal behavior and melting/solidification mechanism during selective laser melting of TiC/Inconel 718 composites, Opt. Laser Technol. 84 (2016) 9–22. doi:10.1016/j.optlastec.2016.04.009.

[37] P. Franciosa, S. Gerbino, D. Ceglarek, Fixture Capability Optimization for Early-stage Design of Assembly System with Compliant Parts Using Nested Polynomial Chaos Expansion, Procedia CIRP. 41 (2016) 87–92. doi:10.1016/j.procir.2015.12.101.

[38] M. Haider, P. Hubert, L. Lessard, An experimental investigation of class A surface finish of composites made by the resin transfer molding process, Compos. Sci. Technol. 67 (2007) 3176–3186. doi:10.1016/j.compscitech.2007.04.010.

[39] H. Thode, Testing for normality, Marcel Dekker, New York, USA, 2002.

[40] J.H. Friedman, Multivariate Adaptive Regression Splines, Ann. Stat. 19 (1991) 1–67. doi:10.1214/aos/1176347963.

[41] T.S. Lee, C.C. Chiu, Y.C. Chou, C.J. Lu, Mining the customer credit using classification and regression tree and multivariate adaptive regression splines, Comput. Stat. Data Anal. 50 (2006) 1113–1130.

[42] G. Jekabsons, ARESLab Adaptive Regression Splines toolbox for Matlab/Octave ver. 1.13.0 User's manual, (2016). http://www.cs.rtu.lv/jekabsons/ (accessed November 28, 2016).

[43] R.B. Dean, W.J. Dixon, Simplified statistics for small numbers of observations, Anal. Chem. 23 (1951) 636–638. http://pubs.acs.org/doi/abs/10.1021/ac60052a025.

[44] E.M. Anawa, A.G. Olabi, Using Taguchi method to optimize welding pool of dissimilar laser-welded components, Opt. Laser Technol. 40 (2008) 379–388. doi:10.1016/j.optlastec.2007.07.001.

[45] Y. Zhao, Y. Zhang, W. Hu, X. Lai, Optimization of laser welding thin-gage galvanized steel via response surface methodology, Opt. Lasers Eng. 50 (2012) 1267–1273. doi:10.1016/j.optlaseng.2012.03.010.

[46] Y. Rong, Z. Zhang, G. Zhang, C. Yue, Y. Gu, Y. Huang, C. Wang, X. Shao, Parameters optimization of laser brazing in crimping butt using Taguchi and BPNN-GA, Opt. Lasers Eng. 67 (2015) 94–104. doi:10.1016/j.optlaseng.2014.10.009.

[47] Z. Gao, X. Shao, P. Jiang, L. Cao, Q. Zhou, C. Yue, Y. Liu, C. Wang, Parameters optimization of hybrid fiber laser-arc butt welding on 316L stainless steel using Kriging model and GA, Opt. Laser Technol. 83 (2016) 153–162. doi:10.1016/j.optlastec.2016.04.001.

Fig. 1. Micro-section of laser welded joint with laser dimpling technique

Fig. 2. (a) Illustration of humping effect during a dimpling process **(b)** dimple upper surface **(c)** dimple lower surface

Fig. 3. Conceptual representation deterministic and stochastic scenarios; **(a)** Experimental results **(b)** Success rate models **(c)** Tolerance limits

Fig. 4. Overview of the experimental setup **(a)** Beam quality measurement **(b)** Laser Dimpling setup (first series of experiments) **(c)** Remote Laser Welding setup (second series of experiments)

Fig. 5. (a) Experimental setup for profilometer **(b)** An example of 3D reconstruction. Process parameters: S_S: 2 m/min, F_O: 35 mm, □: 20°, L_T: 4 mm

Fig. 6. Measurement of the dimple lower surface area **(a)** Grabbed image with scale bar. **(b)** Dimple lower surface area (D_L) for experiment configuration 19 with 5 replications. Process parameters: S_S: 2 m/min, F_O: 25 mm, □: 10°, L_T: 4 mm

Fig. 7. The estimated dimple height value (D_H) over KCC–space in the deterministic scenario

Fig. 8. The estimated dimple upper surface value (D_U) over KCC–space in the deterministic scenario

Fig. 9. The estimated dimple lower surface value (D_L) over KCC–space in the deterministic scenario

Fig. 10. Effect of focal offset on three KPIs when process parameters are constant at S_S: 3 m/min, □: 10°, L_T: 3 mm. (Upper Surface) Surface profilometer results – (Lower Surface) Image processing results

Fig. 11. Deterministic Process Capability Space (**DC_P – Space**) for laser dimpling process

Fig. 12. Stochastic Process Capability Space (**SCP – Space**) for laser dimpling process

Fig. 13 Remote laser welded joint. (**a**) – Trial and error approach before optimization. (**b**) – Optimized configuration based on the proposed methodology